

# PVI: Plug-in Visual Injection for Vision-Language-Action Models

Ze Zhou Zhang, Songxin Zhang, Xiao Xiong, Junjie Zhang, Zejian Xie, Jingyi Xi, Zunyao Mao, Zan Mao, Zhixin Mai, Zhuoyang Song<sup>†</sup>, and Jiaxing Zhang<sup>†</sup>

Lionrock AI Lab, China Merchants Group, Hong Kong, China  
 zezhou.zhang@alumni.pku.edu.cn

<sup>†</sup>Corresponding authors: {songzhuoyang, zhangjiaxing}@cmhk.com

**Abstract.** VLA architectures that pair a pretrained VLM with a flow-matching action expert have emerged as a strong paradigm for language-conditioned manipulation. Yet the VLM, optimized for semantic abstraction and typically conditioned on static visual observations, tends to attenuate fine-grained geometric cues and often lacks explicit temporal evidence for the action expert. Prior work mitigates this by injecting auxiliary visual features, but existing approaches either focus on static spatial representations or require substantial architectural modifications to accommodate temporal inputs, leaving temporal information underexplored. We propose Plug-in Visual Injection (PVI), a lightweight, encoder-agnostic module that attaches to a pretrained action expert and injects auxiliary visual representations via zero-initialized residual pathways, preserving pretrained behavior with only single-stage fine-tuning. Using PVI, we obtain consistent gains over the base policy and a range of competitive alternative injection strategies, and our controlled study shows that temporal video features (V-JEPA2) outperform strong static image features (DINOv2), with the largest gains on multi-phase tasks requiring state tracking and coordination. Real-robot experiments on long-horizon bimanual cloth folding further demonstrate the practicality of PVI beyond simulation.

**Keywords:** Vision-Language-Action Models · Visual Enhancement · Temporal Video Representations

## 1 Introduction

Vision-Language-Action (VLA) models offer a scalable pathway toward generalist robot manipulation by unifying language comprehension with visuomotor control [3, 17, 18, 27, 39, 48]. A prevailing design pairs a Vision-Language Model (VLM) for semantic understanding and instruction grounding with a diffusion or flow-matching Transformer as the action expert, which generates continuous action sequences conditioned on the VLM’s representations [5–7, 24, 36, 37]. However, this factorization carries a structural limitation: the VLM’s language backbone, optimized for semantic abstraction rather than geometric fidelity, tends to compress away fine-grained spatial cues—object geometry, edge alignments, and

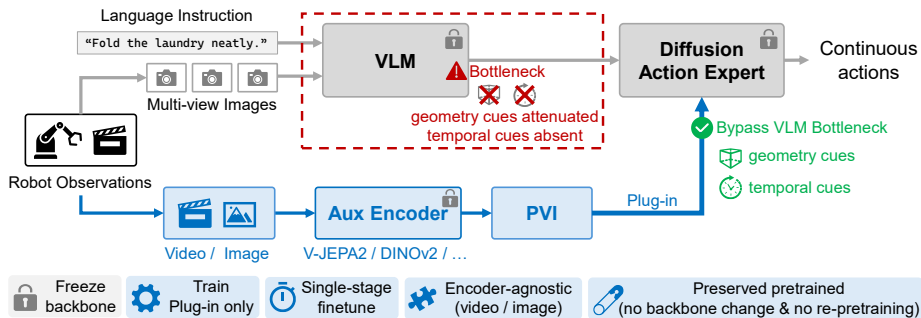


**Fig. 1: Overview of Plug-in Visual Injection (PVI).** Typical VLAs condition the VLM on static images with language, providing limited temporal context; moreover, the VLM’s output representations may under-emphasize fine-grained geometric cues. PVI bypasses this bottleneck by injecting auxiliary visual representations directly into the frozen action expert via a trainable plug-in, with no backbone modification and no re-pretraining required.

grasp affordances—before they ever reach the action expert [23, 26, 39], precisely the information that dexterous manipulation demands.

A natural response to this bottleneck is to enrich the visual information available to the action network beyond what the VLM pathway preserves. Prior work pursues this in two complementary ways: fusing geometry-grounded or spatially enriched features into the VLM’s visual tokens before semantic processing [1, 25], or bypassing the VLM entirely by injecting auxiliary visual representations directly into the action expert via side branches [21–23, 40, 44]. Both strategies recover meaningful geometric detail and have demonstrated improvements in manipulation precision. Yet both strategies share a common limitation: the injected representations are often static, capturing the spatial state of a scene at a single instant while remaining blind to the temporal dynamics—motion continuity, progressive contact, substep transitions—that closed-loop manipulation inherently demands.

Recent work has begun to explore richer temporal and video-based representations within VLA models, demonstrating that motion and contact dynamics provide complementary information beyond static features [28, 32, 41, 46]. However, these approaches typically require substantial architectural modifications to the pretrained backbone or the VLM-to-action interface to accommodate temporal inputs, raising a more fundamental question: how can we inject temporally aware visual information in a way that is lightweight, minimally invasive, and compatible with existing pretrained VLA weights?

We address this challenge with Plug-in Visual Injection (PVI), a lightweight module that injects auxiliary visual representations directly into the flow-matching action expert of a pretrained VLA without modifying its architecture or requiring retraining from scratch, as shown in Fig. 1. PVI introduces a frozen auxiliary visual encoder alongside a trainable copy branch that mirrors the action ex-

per’s architecture and conditioning interface. The copy branch is conditioned on projected auxiliary visual features rather than the VLM representations; its layer-wise hidden states are mapped by zero-initialized injection layers and added residually to the corresponding layers of the frozen main action expert, allowing auxiliary information to influence denoising across the full depth of the policy while preserving pretrained representations. This design enables stable, single-stage fine-tuning through the injection pathway alone. Crucially, the conditioning interface is encoder-agnostic, admitting static, temporal, or combined visual encoders under a unified injection mechanism, decoupling the injection infrastructure from any particular representation choice.

We instantiate PVI on GR00T N1.5 [5] and evaluate it on simulated bimanual manipulation tasks spanning diverse primitives, complemented by real-robot experiments on deformable-object manipulation. Our contributions are three-fold:

- **PVI framework.** We propose Plug-in Visual Injection (PVI), a stable, minimally invasive, and encoder-agnostic visual-injection framework for pretrained VLAs. Via a dual-pathway design with layer-wise zero-initialized residual injection, PVI injects auxiliary representations into a frozen action expert while preserving its pretrained behavior, requiring only single-stage fine-tuning of the injection pathway. Its encoder-agnostic interface admits static, temporal, or combined visual encoders under a unified mechanism, decoupling the injection infrastructure from any particular representation choice.
- **Effective injection via systematic design comparison.** We systematically evaluate PVI against a range of plausible injection strategies across diverse bimanual simulation tasks. PVI improves the average success rate from 35.7% to 59.7% (+24.0 percentage points), outperforming competitive alternatives. Real-robot experiments further validate the effectiveness of PVI beyond simulation, where PVI successfully drives long-horizon bimanual cloth folding that demands precise two-arm coordination over a highly deformable object.
- **Representation study.** Leveraging PVI as a controlled testbed, we systematically compare temporal video encoders, static image encoders, and their combinations. Temporal video features (V-JEPA2 [2]) consistently yield larger gains than strong static baselines (DINOv2 [31]), especially on tasks requiring state tracking and multi-phase coordination, providing direct empirical evidence that temporal dynamics carry complementary information beyond what static representations can supply.

## 2 Related Works

### 2.1 VLA Models with Diffusion/Flow-Matching Action Experts

Early VLAs cast action generation as autoregressive token prediction, inheriting the semantic generalization of large VLMs but relying on action discretization, which can limit fine-grained continuous control [8, 13, 17, 18, 48]. Recent

methods therefore increasingly pair a VLM for semantic grounding with a dedicated diffusion or flow-matching action expert for continuous action generation [5–7,12,24,27,36]. While this design improves action modeling, it also creates a structural bottleneck: the action expert receives visual information primarily through compact VLM representations optimized for semantic abstraction, which can attenuate the precise geometric and temporal cues that dexterous manipulation demands.

## 2.2 Auxiliary Visual Feature Injection

To mitigate this bottleneck, one line of work enriches the VLM pathway itself, fusing geometry-grounded or spatially enriched features into VLM visual representations before semantic processing, or strengthening the vision backbone with pretrained geometric and spatiotemporal priors [1, 14, 25, 28, 33, 41, 45, 46]. However, because the enriched signal is still mediated by the VLM, it remains subject to semantic compression before reaching the action expert. A more direct approach bypasses the VLM entirely by injecting auxiliary visual features into the action expert through side branches, inspired by side-branch conditioning paradigms from conditional generation [16, 29, 42]. Recent VLA variants have validated this strategy by injecting object-centric or 3D geometric features into pretrained action experts [21–23, 44]. Yet existing methods are largely designed around specific static encoders and task-specific augmentation, leaving open the question of how to build a stable, minimally invasive, and encoder-agnostic injection interface that preserves pretrained capabilities while enabling systematic comparison across different visual representations, including temporal ones.

## 2.3 Visual Representations for Manipulation: From Static to Temporal

Existing visual injection methods for VLAs often rely on static spatial representations, including object-centric features, point-cloud or geometric cues, and single-frame image embeddings, which are effective for target localization and scene layout encoding [10, 15, 19, 21–23, 30, 34, 35, 40, 44]. Yet in fine-grained manipulation, especially bimanual, multi-stage, and partially observable settings, the policy must also infer motion progression, alignment convergence, contact transitions, and subtask completion, signals that are inherently ambiguous from a single observation. Temporal representations have been studied across video modeling, robot learning, and VLA models through predictive video representation learning, recurrent policies, world models, and video-based conditioning, demonstrating that motion and contact dynamics provide complementary information beyond static features [2, 4, 9, 20, 28, 32, 38, 41, 43, 46, 47]. However, these approaches typically require substantial architectural modifications to accommodate temporal inputs, leaving temporal representations largely unexplored as lightweight injected conditions for pretrained action experts. PVI directly targets this gap by providing an encoder-agnostic injection interface that decouples the choice of visual representation from the pretrained action expert, enabling a

principled study of temporal dynamics as a complementary signal for dexterous manipulation.

### 3 Method

#### 3.1 Preliminaries

**VLA Architecture with a Flow-Matching Action Expert.** We consider a typical VLA architecture composed of two parts: a vision-language model (VLM) backbone for semantic grounding and a Diffusion Transformer (DiT) action expert for continuous action generation. Given a language instruction  $l$  and multi-view image observations  $\{I_v\}_{v=1}^V$ , the VLM jointly encodes them into a sequence of embeddings

$$\mathbf{z}_{v1} \in \mathbb{R}^{S \times D}, \quad (1)$$

where  $S$  is the sequence length and  $D$  is the embedding dimension.

**Flow-Matching Action Generation.** The DiT action expert learns a velocity field  $\hat{v}_\theta$  that transports Gaussian noise to the target action trajectory. Let  $\mathbf{a} = (\mathbf{a}_1, \dots, \mathbf{a}_H)$  denote the target action sequence of horizon  $H$ , and let  $\epsilon \sim \mathcal{N}(\mathbf{0}, \mathbf{I})$ . At flow time  $t \in [0, 1]$ , the interpolated trajectory is

$$\mathbf{a}_t = (1 - t)\epsilon + t\mathbf{a}. \quad (2)$$

Conditioned on  $\mathbf{z}_{v1}$ , the DiT predicts the velocity field and is trained with the standard flow-matching objective

$$\mathcal{L} = \mathbb{E}_{t, \epsilon} \left[ \left\| \hat{v}_\theta(\mathbf{a}_t, t, \mathbf{z}_{v1}) - (\mathbf{a} - \epsilon) \right\|_2^2 \right]. \quad (3)$$

At inference time, the model generates actions by integrating the predicted velocity field from pure noise using  $K$ -step Euler updates.

**The Semantic-Geometric and Temporal Gap.** In this architecture,  $\mathbf{z}_{v1}$  is the sole channel through which visual information reaches the action expert. However, VLMs are primarily optimized for high-level semantic understanding, such as language alignment and scene-level reasoning. As a result, their embeddings do not reliably preserve fine-grained geometric cues (e.g., edges, local depth, contact surfaces) or temporal dynamics (e.g., motion trends and state transitions) that are critical for dexterous manipulation. This bottleneck is especially severe in bimanual tasks requiring sub-centimeter precision.

To address this, we propose PVI, a lightweight plug-in module that injects auxiliary visual representations directly into the frozen action expert.

#### 3.2 PVI: Architecture Overview

PVI augments a pretrained VLA with a side-branch visual injection pathway, while keeping the original architecture and pretrained knowledge intact, as shown in Fig. 2. The key idea is to inject fine-grained auxiliary visual features directly into the DiT action generation process, rather than relying solely on the VLM embedding. PVI consists of three components:

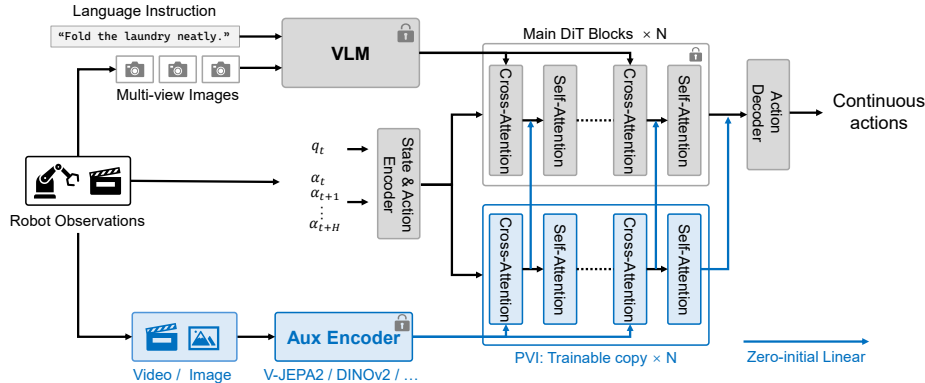


**Fig. 2: Architecture overview.** The frozen main DiT blocks receive semantic embeddings from a frozen VLM. A trainable DiT copy (PVI) conditions on auxiliary visual features and injects them into the main stream via zero-initialized linear projections to produce continuous actions.

- **Encoder-agnostic auxiliary visual feature extraction.** A frozen auxiliary visual encoder  $E$  extracts features  $\mathbf{z}_{\text{aux}}$  from raw observations. A trainable zero-initialized projection maps these features into the DiT embedding space. PVI imposes no restriction on the choice of  $E$ , enabling plug-and-play integration of heterogeneous visual representations.
- **Copy-branch DiT with dual conditioning and layer-wise injection.** We instantiate a trainable copy branch that mirrors the architecture of the main DiT and is initialized from its pretrained weights. The copy branch retains the same conditioning mechanism as the main DiT, but substitutes the VLM condition  $\mathbf{z}_{v_l}$  with the projected auxiliary features  $\tilde{\mathbf{z}}_{\text{aux}}$ . Its layer-wise hidden states are injected into the frozen main DiT through zero-initialized residual mappings.
- **Zero-initialized training with minimal intervention.** We freeze the VLM and the main DiT, and train only the newly introduced projection, copy branch, and injection layers (plus embodiment-specific state/action adapters when applicable). Zero initialization ensures that training starts from behavior equivalent to the original pretrained VLA and gradually incorporates auxiliary visual information.

We describe these components in detail below.

### 3.3 Encoder-Agnostic Auxiliary Visual Feature Extraction

PVI does not assume a specific auxiliary visual encoder. We only require an encoder  $E$  that takes raw observations as input and outputs a fixed-dimensional feature sequence  $\mathbf{z}_{\text{aux}} \in \mathbb{R}^{L \times d_E}$ , where  $L$  is the auxiliary sequence length and  $d_E$  is the encoder feature dimension. A trainable linear projection  $\mathbf{W}_{\text{proj}} \in \mathbb{R}^{d_E \times D}$

maps these features into the DiT embedding space:

$$\tilde{\mathbf{z}}_{\text{aux}} = \mathbf{z}_{\text{aux}} \mathbf{W}_{\text{proj}} \in \mathbb{R}^{L \times D}. \quad (4)$$

We initialize  $\mathbf{W}_{\text{proj}}$  to zero so that the copy branch receives a zero conditioning signal at the start of training.

This encoder-agnostic design enables controlled comparison across different classes of visual representations, each compensating for a different limitation of  $\mathbf{z}_{\text{vl}}$ . In this work, we focus on two complementary categories:

- **Temporal dynamic representations**, extracted from video clips, which encode motion trajectories and state evolution and compensate for the lack of temporal dynamics in static VLM embeddings.
- **Spatial geometric representations**, extracted from image observations, which encode boundaries, depth cues, and fine spatial structure and compensate for geometric information loss caused by semantic compression in the VLM.

### 3.4 Dual-Pathway DiT with Layer-wise Injection

**Shared Initial Features.** Let the main DiT contain  $N$  Transformer blocks. A proprioceptive state and noisy action tokens are first encoded and concatenated into an initial token sequence  $\mathbf{h}_0 \in \mathbb{R}^{M \times D}$ , where  $M$  is the number of tokens and  $D$  is the hidden dimension. This same  $\mathbf{h}_0$  is used as input to both the frozen main DiT and the trainable copy branch.

**Dual Conditioning.** In a common DiT action expert, each Transformer block receives the VLM embedding  $\mathbf{z}_{\text{vl}}$  through an architecture-dependent conditioning mechanism (e.g., cross-attention, AdaLN modulation, or conditional concatenation). The copy branch preserves the exact architecture and conditioning mechanism of the main DiT, but replaces  $\mathbf{z}_{\text{vl}}$  with  $\tilde{\mathbf{z}}_{\text{aux}}$  as the conditioning input. This keeps the copy branch structurally aligned with the pretrained action expert while specializing it to process auxiliary visual information.

For example, GR00T N1.5 uses cross-attention layers conditioned on  $\mathbf{z}_{\text{vl}}$  alongside self-attention. In the PVI copy branch, the same cross-attention structure is retained, but its key/value inputs are replaced by  $\tilde{\mathbf{z}}_{\text{aux}}$ . The same principle applies to other conditioning mechanisms.

**Layer-Wise Residual Injection.** Denote the  $i$ -th block of the frozen main DiT by  $f_i^{\text{main}}$  and the corresponding block in the trainable copy branch by  $f_i^{\text{copy}}$ . The copy branch is computed as

$$\mathbf{h}_i^{\text{copy}} = f_i^{\text{copy}}(\mathbf{h}_{i-1}^{\text{copy}}, \tilde{\mathbf{z}}_{\text{aux}}), \quad i = 1, \dots, N. \quad (5)$$

The main DiT is computed in parallel and receives a layer-wise control signal from the copy branch:

$$\mathbf{h}_i^{\text{main}} = f_i^{\text{main}}(\mathbf{h}_{i-1}^{\text{main}}, \mathbf{z}_{\text{vl}}) + \mathbf{Z}_i(\mathbf{h}_i^{\text{copy}}), \quad i = 1, \dots, N, \quad (6)$$

where  $\mathbf{Z}_i$  is a zero-initialized linear injection layer. This design allows auxiliary visual information to influence action generation at every layer of the DiT while preserving the pretrained main pathway.

### 3.5 Training Strategy

We freeze all pretrained components of the original VLA, including the VLM backbone and the main DiT, as well as the auxiliary visual encoder  $E$ . The trainable parameters are the projection layer  $\mathbf{W}_{\text{proj}}$ , the copy-branch blocks  $\{f_i^{\text{copy}}\}_{i=1}^N$ , the injection layers  $\{\mathbf{Z}_i\}_{i=1}^N$ , and embodiment-specific state/action encoders and decoders that bridge the target embodiment to the pretrained VLA interface.

The copy branch is initialized by copying the pretrained weights of the main DiT, providing a strong feature-processing prior from the start of training. The projection layer  $\mathbf{W}_{\text{proj}}$  and injection layers  $\{\mathbf{Z}_i\}_{i=1}^N$  are initialized to zero, which guarantees functional equivalence to the original pretrained VLA at initialization: the auxiliary pathway produces zero control signals and does not perturb the frozen main pathway. As training proceeds, the injection layers learn non-zero mappings, enabling gradual integration of auxiliary visual information and reducing the risk of interference with pretrained knowledge.

PVI uses the same flow-matching loss as the baseline and introduces no auxiliary supervision. All newly introduced parameters are trained solely through the action prediction objective.

## 4 Experiments

To validate PVI, we instantiate it on GR00T N1.5 using the released pretrained model as our base. We begin with a quantitative comparison of candidate injection strategies in simulation to evaluate whether PVI provides a stronger mechanism for delivering auxiliary visual information to the flow-matching action expert (Sec. 4.1). We then demonstrate encoder-agnostic generality by plugging in different auxiliary encoders and conducting a controlled representation study that compares temporal and spatial visual features, as well as their combinations (Sec. 4.2). Next, we analyze key design choices through ablations on temporal context length and stabilization options (Sec. 4.3), and evaluate PVI under a more challenging multi-task regime (Sec. 4.4). Finally, we provide a qualitative real-robot demonstration on bimanual cloth folding, a long-horizon task requiring precise two-arm coordination over a deformable object, to validate the practicality of deploying PVI beyond simulation (Sec. 4.5).

Across all simulation experiments, we enforce a consistent training and evaluation protocol for fair comparison. All methods, including the baseline GR00T N1.5, GR00T N1.5 + PVI, and other candidate injection strategies, start from the same pretrained weights and undergo a single round of fine-tuning on the same task data, with identical training steps, learning rate, batch size, and all other hyperparameters. The only difference across conditions is the injection architecture and the associated freezing strategy. Full implementation details for all variants (architectures, freezing policies, trainable parameter counts) and training hyperparameters are provided in the supplementary material.

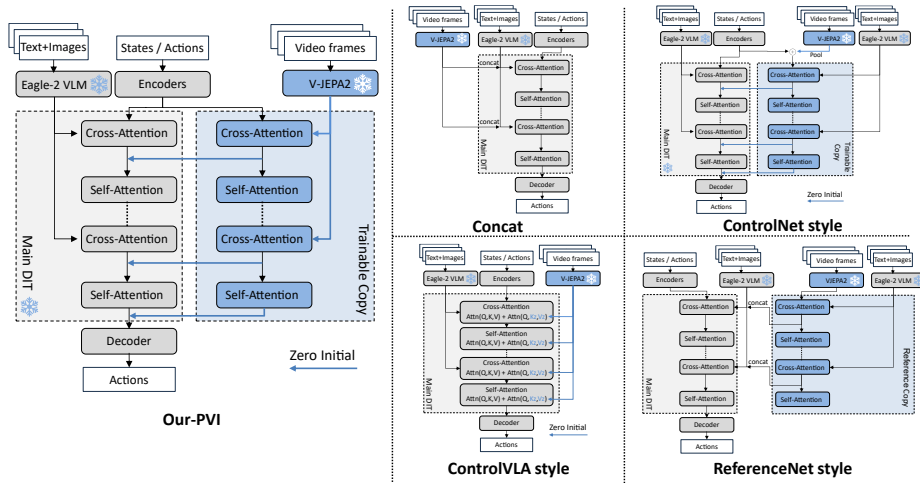


**Fig. 3: Overview of PVI and four candidate strategies for injecting auxiliary visual features into the DiT action expert.** We compare **PVI** (ours), which injects V-JEPA2 features via a trainable copy branch with zero-initialized injection layers, against input-level fusion (**Concat**), attention-level dual injection (**ControlVLA-style**), and parallel-branch designs with feature concatenation or residual addition (**ReferenceNet-** and **ControlNet-style**).

#### 4.1 Comparing Injection Strategies

We compare PVI against several candidate strategies for injecting auxiliary visual information into a pretrained flow-matching action expert. We draw inspiration from related domains to instantiate four plausible injection designs: **Concat** represents a natural baseline; **ControlNet-** and **ReferenceNet-style** strategies adapt conditioning mechanisms from text-to-image generation [16, 42]; and **ControlVLA-style** adapts the zero-initialized dual cross-attention mechanism from ControlVLA [23], which was originally proposed for injecting object-centric features into pretrained VLA models. To isolate the effect of the injection mechanism, we fix the auxiliary encoder to V-JEPA2 and the training budget across all methods and vary only how auxiliary features are introduced into the action expert (Fig. 3).

We consider four alternative designs:

(1) **Concat-style** concatenates auxiliary visual embeddings with VLM representations as the joint cross-attention key/value context for the DiT. Since the action expert must learn to interpret the expanded context, the full DiT is fine-tuned end-to-end.

(2) **ControlNet-style** maintains a trainable copy of the frozen action expert, where auxiliary visual features are added to the state-action embeddings before entering the control branch. The control branch also receives VLM representations as cross-attention conditioning, and injects its intermediate representations into the frozen main DiT via zero-initialized residual additions at each block.

**Table 1: Comparing injection strategies in simulation (single-task fine-tuning).** Success rates (%) over 100 evaluation rollouts per task with randomized initial conditions (different rollout seeds). Evaluated tasks span diverse manipulation primitives, including alignment and perception, press and switch, relocation and placement, articulation, and coordination with tools and stacking.

Task	GR00T N1.5	Ours	Concat	ControlNet	ControlVLA	ReferenceNet
adjust_bottle	92	95	90	86	91	<b>96</b>
beat_block_hammer	39	<b>84</b>	47	30	35	37
click_alarmclock	48	<b>87</b>	54	46	53	48
move_can_pot	37	<b>51</b>	36	30	37	37
click_bell	46	<b>91</b>	75	41	61	42
move_playingcard_away	23	<b>84</b>	39	29	26	61
pick_diverse_bottles	3	<b>24</b>	4	10	4	5
place_a2b_left	31	<b>36</b>	31	21	28	19
open_laptop	48	70	<b>71</b>	38	53	61
press_stapler	31	<b>72</b>	43	52	31	41
rotate_qrcode	38	<b>55</b>	45	26	36	46
scan_object	4	<b>42</b>	14	18	10	15
put_object_cabinet	24	<b>36</b>	18	22	23	21
turn_switch	28	<b>62</b>	25	57	27	27
handover_block	21	<b>50</b>	45	27	24	28
open_microwave	38	51	<b>54</b>	34	46	49
stack_blocks_two	40	<b>60</b>	49	19	25	23
stack_bowls_two	79	86	85	76	<b>89</b>	73
blocks_ranking_rgb	33	<b>43</b>	32	21	34	12
blocks_ranking_size	11	<b>15</b>	<b>15</b>	4	7	7
<b>Average success</b>	35.70	<b>59.70</b>	43.60	34.35	37.00	37.40
$\Delta$ vs. Base (pp)	–	<b>+24.00</b>	+7.90	–1.35	+1.30	+1.70

(3) **ReferenceNet-style** similarly uses a parallel DiT copy, but replaces the state-action embedding input entirely with auxiliary visual features while retaining VLM conditioning. Unlike ControlNet-style, both the main DiT and the reference branch are trained jointly, incurring higher training cost.

(4) **ControlVLA-style** injects auxiliary features directly at the attention computation level: an auxiliary attention term  $\text{softmax}(QK_z^T/\sqrt{d})V_z$  is added alongside the standard attention, where  $K_z, V_z$  are zero-initialized projections of the auxiliary features. The full DiT and auxiliary projections are optimized jointly.

We conduct a quantitative evaluation in RoboTwin 2.0 [11], a bimanual manipulation simulator covering diverse task types and manipulation primitives. Following the shared protocol described above, we fine-tune each method independently on each task using 50 demonstration trajectories and report success rates over 100 evaluation rollouts with randomized initial conditions. Unless otherwise stated, all methods use a frozen V-JEPA2 encoder taking 8 frames sampled at 4 fps as the auxiliary feature source.

Tab. 1 summarizes results across 20 bimanual tasks. The fine-tuned GR00T N1.5 baseline achieves **35.7%** average success, while GR00T N1.5 + PVI reaches **59.7%** (+**24.0** pp). Concat provides a moderate improvement (**43.6%**), whereas the ControlVLA-, ControlNet-, and ReferenceNet-style variants remain close to the baseline (**34.4–37.4%**). PVI’s gains are particularly pronounced on tasks

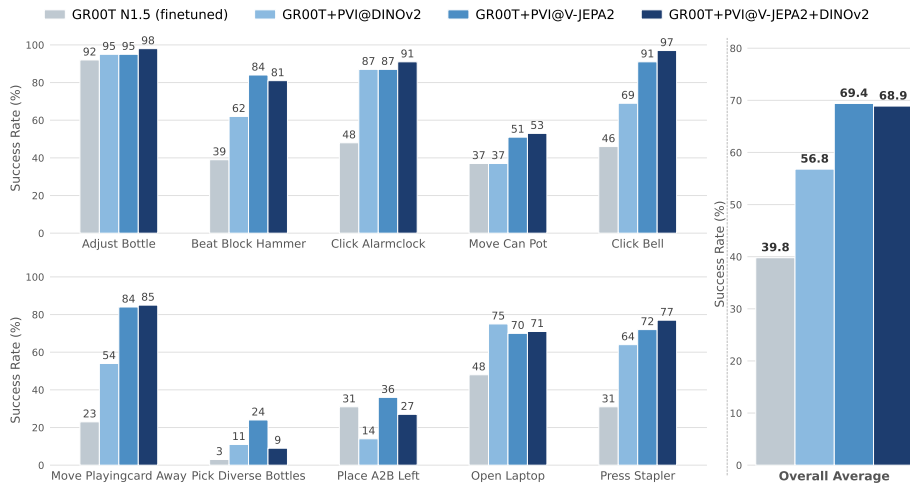


**Fig. 4: Encoder-agnostic visual injection and representation comparison.** Per-task success rates and overall average across 10 simulation tasks, comparing a fine-tuned GR00T N1.5 baseline against three PVI instantiations with different auxiliary encoders.

with low baseline success, for example `beat_block_hammer` (39%  $\rightarrow$  84%), `click_alarmclock` (48%  $\rightarrow$  87%), `move_playingcard_away` (23%  $\rightarrow$  84%), and `scan_object` (4%  $\rightarrow$  42%). These results support two conclusions: injecting temporal evidence into the action expert is broadly beneficial for contact-rich bimanual manipulation, and the injection mechanism itself matters significantly. PVI’s dual-conditioning and behavior-preserving layer-wise injection yield substantially larger gains than competing designs under the same data and training budget.

## 4.2 Encoder-Agnostic Injection and Representation Study

Having established that the injection mechanism matters, we next study what auxiliary visual information should be injected. A key advantage of PVI is its encoder-agnostic interface: the same injection pathway can accept heterogeneous auxiliary encoders without architectural changes to the pretrained action expert. This enables two goals under a unified setup: (i) validating that PVI can plug in different representations and consistently improve a strong base VLA, and (ii) conducting a controlled comparison where the injected representation is the primary variable.

We evaluate on 10 simulation tasks from RoboTwin 2.0 following the same protocol described in Sec. 4.1. We denote GR00T augmented with PVI and an auxiliary encoder  $E$  as GR00T+PVI@ $E$ , and compare three instantiations: GR00T+PVI@DINOv2, which injects static image features from a single frame; GR00T+PVI@V-JEPA2, which injects temporal video features from 8 frames

sampled at 4 fps; and GR00T+PVI@V-JEPA2+DINOv2, which combines both encoders through the same interface.

Results are shown in Fig. 4. The fine-tuned GR00T N1.5 baseline achieves **39.8%** average success. All three PVI instantiations consistently improve over the baseline, confirming that the encoder-agnostic interface transfers benefit regardless of the encoder type. Injecting static features already yields a substantial gain: GR00T+PVI@DINOv2 reaches **56.8%** (+**17.0** pp, +**42.7%** relative). Temporal features provide the largest improvement: GR00T+PVI@V-JEPA2 reaches **69.4%** (+**29.6** pp, +**74.4%** relative). Combining both encoders achieves **68.9%** (+**29.1** pp, +**73.1%** relative), on par with V-JEPA2 alone, suggesting that static appearance features provide little additional signal beyond what temporal features already capture. The consistent advantage of temporal features across tasks, particularly those involving multi-phase coordination and state tracking, points to temporally coherent evidence as the more critical ingredient for closed-loop bimanual manipulation.

### 4.3 Ablations and Sensitivity Analysis

We analyze the sensitivity of PVI to temporal context length and stabilization/adaptation choices. All ablations follow the same protocol and use 10 simulation tasks from RoboTwin 2.0 as in Sec. 4.2, reporting average success over 100 rollouts per task. Results are summarized in Tab. 2.

Varying the number of frames fed to the frozen V-JEPA2 encoder at 4 fps, we find that a moderate temporal context is sufficient: 2–4 frames achieve the best performance (**71.6%**–**71.8%**), while longer contexts yield diminishing returns (**69.4%** at 8 frames, **66.6%** at 16 frames). Notably, the default 8-frame setting used throughout our main experiments is not the optimal configuration identified here; the performance gap is small (2.4 pp) but suggests that the gains reported in Sec. 4.1 and Sec. 4.2 are conservative, and that PVI can be further improved with task-specific tuning of temporal context. Combining temporal and static encoders through the same interface yields competitive performance (**68.9%** with V-JEPA2+DINOv2 at 16 frames), suggesting limited additional benefit beyond temporal features alone.

We further ablate stabilization and adaptation choices. Freezing the auxiliary-to-DiT projector substantially reduces performance (**55.3%**), indicating that learning feature alignment into the action expert’s embedding space is important even when the auxiliary encoder is frozen. Removing zero initialization yields comparable or slightly higher final success (**71.8%**); nevertheless, we retain zero initialization in our main experiments because it guarantees behavior-preserving initialization and supports conservative, progressive integration of auxiliary signals during fine-tuning.

### 4.4 Multi-Task Scalability

We further evaluate PVI in a multi-task regime, where a single policy must cover a broad set of skills while sharing the same action expert across tasks. We

**Table 2: Ablations on temporal context and stabilization choices.** Average success rates (%) over 100 evaluation rollouts per task with randomized initial conditions (different rollout seeds).

Variant	Frames@4fps	Avg. (%)
Baseline (fine-tuned GR00T N1.5)	–	39.8
<i>Temporal context (PVI@V-JEPA2)</i>		
PVI@V-JEPA2	2	71.6
PVI@V-JEPA2	4	71.8
PVI@V-JEPA2	8	69.4
PVI@V-JEPA2	16	66.6
PVI@V-JEPA2 + DINOv2	16	68.9
<i>Stabilization / adaptation (PVI@V-JEPA2, 8f)</i>		
PVI@V-JEPA2 (no zero-init)	8	71.8
PVI@V-JEPA2 (freeze projector)	8	55.3

train on a 20-task and a 50-task RoboTwin 2.0 mixture with 50 demonstrations per task, starting from the same pretrained GR00T N1.5 checkpoint. We report per-task success rates over 100 rollouts and summarize performance by average success rate.

PVI consistently improves over the fine-tuned GR00T N1.5 baseline in both settings. On the 20-task mixture, PVI increases average success from 61.15% to 69.15% (+8.00 pp). On the more challenging 50-task mixture, PVI yields a consistent gain from 61.32% to 63.56% (+2.24 pp), winning on the majority of individual tasks. These results suggest that auxiliary visual injection remains beneficial even when training a shared policy over diverse manipulation primitives. Full per-task results are provided in the supplementary material.

#### 4.5 Real-World Bimanual Deformable-Object Demonstration

To assess the practicality of PVI beyond simulation, we deploy it on an Airbot dual-arm platform for long-horizon bimanual cloth folding—a task that demands precise two-arm coordination, contact-rich interaction, and sustained shape reasoning over a highly deformable garment. We collect a set of demonstration trajectories and fine-tune the GR00T N1.5 checkpoint with PVI attached, following the same single-stage fine-tuning procedure as in simulation without any task-specific engineering.

The resulting policy executes a full eight-stage folding sequence in closed loop, driven by language instructions without manual resets between subtasks. As shown in Fig. 5, the policy handles the diverse manipulation primitives required by the task—precise pinching, global shape adjustment, symmetric bimanual coordination, and contact-rich sliding with tension control—across all eight stages. This demonstration provides qualitative evidence that PVI can be

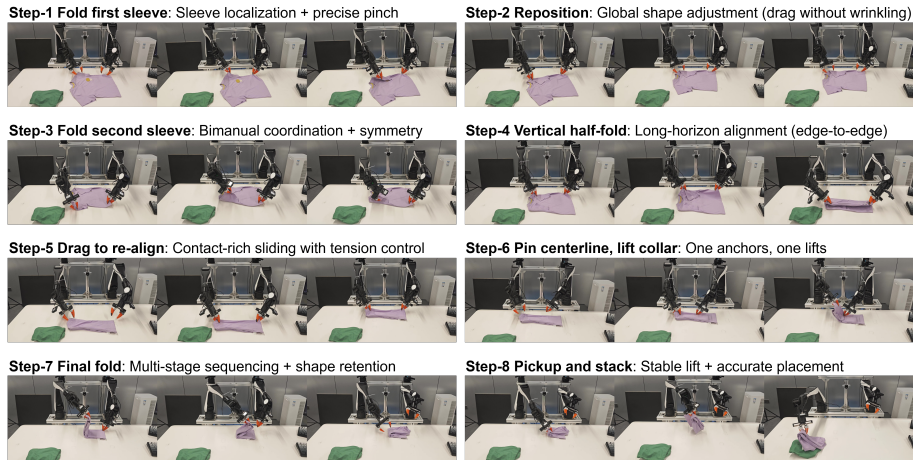


**Fig. 5: PVI enables long-horizon bimanual manipulation of deformable objects on real hardware.** The task comprises eight sequential subtasks, each illustrated by three keyframes: sleeve localization and precise pinching (Step 1), global shape adjustment via dragging without wrinkling (Step 2), symmetric bimanual sleeve folding (Step 3), long-horizon edge-to-edge vertical half-fold (Step 4), contact-rich sliding with tension control (Step 5), asymmetric anchoring and collar lifting (Step 6), multi-stage final fold with shape retention (Step 7), and stable lift-and-stack (Step 8). All subtasks are driven by a single PVI-augmented policy conditioned on language instructions, without task-specific engineering or manual resets between steps.

fine-tuned and deployed on real bimanual hardware and remains effective for challenging long-horizon deformable-object manipulation.

## 5 Conclusion

We presented Plug-in Visual Injection (PVI), a lightweight, encoder-agnostic framework that injects auxiliary visual representations directly into the frozen action expert of a pretrained VLA via a behavior-preserving, layer-wise residual pathway, enabling stable single-stage fine-tuning without any backbone modification. Across a broad suite of bimanual manipulation tasks, PVI substantially improves over a fine-tuned GR00T N1.5 baseline and outperforms a range of competitive injection strategies, demonstrating that *how* auxiliary information is injected is as important as *what* is injected. Using PVI as a controlled testbed, we further show that temporal video representations outperform strong static image features for fine-grained multi-phase manipulation, with the largest gains on tasks requiring state tracking and cross-arm coordination. PVI scales to multi-task regimes and transfers to real bimanual hardware for long-horizon deformable-object manipulation, establishing a simple and stable foundation for integrating richer visual signals into future VLA systems.

## Acknowledgements

We thank Dong Sun and Chaorong Zhang for their contributions to bimanual real-robot data collection and processing, and Ting Sun for his contributions to the training framework.

## References

1. Abouzeid, A., Mansour, M., Sun, Z., Song, D.: Geoaware-vla: Implicit geometry aware vision-language-action model. arXiv preprint arXiv:2509.14117 (2025)
2. Assran, M., Bardes, A., Fan, D., Garrido, Q., Howes, R., Muckley, M., Rizvi, A., Roberts, C., Sinha, K., Zhohus, A., et al.: V-jepa 2: Self-supervised video models enable understanding, prediction and planning. arXiv preprint arXiv:2506.09985 (2025)
3. Bai, S., Song, W., Chen, J., Ji, Y., Zhong, Z., Yang, J., Zhao, H., Zhou, W., Zhao, W., Li, Z., et al.: Towards a unified understanding of robot manipulation: A comprehensive survey. arXiv preprint arXiv:2510.10903 (2025)
4. Bi, H., Tan, H., Xie, S., Wang, Z., Huang, S., Liu, H., Zhao, R., Feng, Y., Xiang, C., Rong, Y., et al.: Motus: A unified latent action world model. arXiv preprint arXiv:2512.13030 (2025)
5. Bjorck, J., Castañeda, F., Cherniadev, N., Da, X., Ding, R., Fan, L., Fang, Y., Fox, D., Hu, F., Huang, S., et al.: Gr00t n1: An open foundation model for generalist humanoid robots. arXiv preprint arXiv:2503.14734 (2025)
6. Black, K., Brown, N., Darpinian, J., Dhabalia, K., Driess, D., Esmail, A., Equi, M.R., Finn, C., Fusai, N., Galliker, M.Y., et al.:  $\pi_{0.5}$ : a vision-language-action model with open-world generalization. In: 9th Annual Conference on Robot Learning (2025)
7. Black, K., Brown, N., Driess, D., Esmail, A., Equi, M., Finn, C., Fusai, N., Groom, L., Hausman, K., Ichter, B., et al.:  $\pi_0$ : A vision-language-action flow model for general robot control. arXiv preprint arXiv:2410.24164 (2024)
8. Brohan, A., Brown, N., Carbajal, J., Chebotar, Y., Dabis, J., Finn, C., Gopalakrishnan, K., Hausman, K., Herzog, A., Hsu, J., Ibarz, J., Ichter, B., Irpan, A., Jackson, T., Jesmonth, S., Joshi, N., Julian, R., Kalashnikov, D., Kuang, Y., Leal, I., Lee, K.H., Levine, S., Lu, Y., Malla, U., Manjunath, D., Mordatch, I., Nachum, O., Parada, C., Peralta, J., Perez, E., Pertsch, K., Quiambao, J., Rao, K., Ryoo, M., Salazar, G., Sanketi, P., Sayed, K., Singh, J., Sontakke, S., Stone, A., Tan, C., Tran, H., Vanhoucke, V., Vega, S., Vuong, Q., Xia, F., Xiao, T., Xu, P., Xu, S., Yu, T., Zitkovich, B.: Rt-1: Robotics transformer for real-world control at scale. In: arXiv preprint arXiv:2212.06817 (2022)
9. Chen, D., Shukor, M., Moutakanni, T., Chung, W., Yu, J., Kasarla, T., Bolourchi, A., LeCun, Y., Fung, P.: Vl-jepa: Joint embedding predictive architecture for vision-language. arXiv preprint arXiv:2512.10942 (2025)
10. Chen, S., Liu, J., Qian, S., Jiang, H., Li, L., Zhang, R., Liu, Z., Gu, C., Hou, C., Wang, P., et al.: Ac-dit: Adaptive coordination diffusion transformer for mobile manipulation. arXiv preprint arXiv:2507.01961 (2025)
11. Chen, T., Chen, Z., Chen, B., Cai, Z., Liu, Y., Li, Z., Liang, Q., Lin, X., Ge, Y., Gu, Z., et al.: Robotwin 2.0: A scalable data generator and benchmark with strong domain randomization for robust bimanual robotic manipulation. arXiv preprint arXiv:2506.18088 (2025)

12. Chi, C., Xu, Z., Feng, S., Cousineau, E., Du, Y., Burchfiel, B., Tedrake, R., Song, S.: Diffusion policy: Visuomotor policy learning via action diffusion. *The International Journal of Robotics Research* **44**(10-11), 1684–1704 (2025)
13. Driess, D., Xia, F., Sajjadi, M.S., et al.: Palm-e: An embodied multimodal language model. In: *Proceedings of the 40th International Conference on Machine Learning (ICML)* (2023)
14. Feng, Y., Zhang, W., Wang, Y., Luo, H., Yuan, H., Zheng, S., Lu, Z.: Spatial-aware vla pretraining through visual-physical alignment from human videos. *arXiv preprint arXiv:2512.13080* (2025)
15. Ge, S., Zhang, Y., Xie, S., Zhang, W., Zhou, M., Wang, Z.: Vggt-dp: Generalizable robot control via vision foundation models. *arXiv preprint arXiv:2509.18778* (2025)
16. Hu, L.: Animate anyone: Consistent and controllable image-to-video synthesis for character animation. In: *Proceedings of the IEEE/CVF conference on computer vision and pattern recognition*. pp. 8153–8163 (2024)
17. Kim, M.J., Finn, C., Liang, P.: Fine-tuning vision-language-action models: Optimizing speed and success. *arXiv preprint arXiv:2502.19645* (2025)
18. Kim, M.J., Pertsch, K., Karamcheti, S., Xiao, T., Balakrishna, A., Nair, S., Rafailov, R., Foster, E., Lam, G., Sanketi, P., et al.: Openvla: An open-source vision-language-action model. *arXiv preprint arXiv:2406.09246* (2024)
19. Kirillov, A., Mintun, E., Ravi, N., Mao, H., Rolland, C., Gustafson, L., Xiao, T., Whitehead, S., Berg, A.C., Lo, W.Y., et al.: Segment anything. In: *Proceedings of the IEEE/CVF international conference on computer vision*. pp. 4015–4026 (2023)
20. Koo, M., Choi, D., Kim, T., Lee, K., Kim, C., Seo, Y., Shin, J.: Hamlet: Switch your vision-language-action model into a history-aware policy. *arXiv preprint arXiv:2510.00695* (2025)
21. Li, C., Wen, J., Peng, Y., Peng, Y., Zhu, Y.: Pointvla: Injecting the 3d world into vision-language-action models. *IEEE Robotics and Automation Letters* **11**(3), 2506–2513 (2026)
22. Li, J., Zhu, Y., Tang, Z., Wen, J., Zhu, M., Liu, X., Li, C., Cheng, R., Peng, Y., Peng, Y., et al.: Coa-vla: Improving vision-language-action models via visual-text chain-of-affordance. In: *Proceedings of the IEEE/CVF International Conference on Computer Vision*. pp. 9759–9769 (2025)
23. Li, P., Wu, Y., Xi, Z., Li, W., Huang, Y., Zhang, Z., Chen, Y., Wang, J., Zhu, S.C., Liu, T., et al.: Controlvla: Few-shot object-centric adaptation for pre-trained vision-language-action models. *arXiv preprint arXiv:2506.16211* (2025)
24. Li, Q., Liang, Y., Wang, Z., Luo, L., Chen, X., Liao, M., Wei, F., Deng, Y., Xu, S., Zhang, Y., et al.: Cogact: A foundational vision-language-action model for synergizing cognition and action in robotic manipulation. *arXiv preprint arXiv:2411.19650* (2024)
25. Lin, T., Li, G., Zhong, Y., Zou, Y., Du, Y., Liu, J., Gu, E., Zhao, B.: Evo-0: Vision-language-action model with implicit spatial understanding. *arXiv preprint arXiv:2507.00416* (2025)
26. Liu, J., Chen, H., An, P., Liu, Z., Zhang, R., Gu, C., Li, X., Guo, Z., Chen, S., Liu, M., et al.: Hybridvla: Collaborative diffusion and autoregression in a unified vision-language-action model. *arXiv preprint arXiv:2503.10631* (2025)
27. Liu, S., Wu, L., Li, B., Tan, H., Chen, H., Wang, Z., Xu, K., Su, H., Zhu, J.: Rdt-1b: a diffusion foundation model for bimanual manipulation. *arXiv preprint arXiv:2410.07864* (2024)
28. Miao, S., Feng, N., Wu, J., Lin, Y., He, X., Li, D., Long, M.: Jepa-vla: Video predictive embedding is needed for vla models. *arXiv preprint arXiv:2602.11832* (2026)

29. Mou, C., Wang, X., Xie, L., Wu, Y., Zhang, J., Qi, Z., Shan, Y.: T2i-adapter: Learning adapters to dig out more controllable ability for text-to-image diffusion models. In: Proceedings of the AAAI conference on artificial intelligence. vol. 38, pp. 4296–4304 (2024)
30. Ni, Z., He, Y., Qian, L., Mao, J., Fu, F., Sui, W., Su, H., Peng, J., Wang, Z., He, B.: Vo-dp: Semantic-geometric adaptive diffusion policy for vision-only robotic manipulation. arXiv preprint arXiv:2510.15530 (2025)
31. Oquab, M., Darcet, T., Moutakanni, T., Vo, H., Szafraniec, M., Khalidov, V., Fernandez, P., Haziza, D., Massa, F., El-Nouby, A., et al.: Dinov2: Learning robust visual features without supervision. arXiv preprint arXiv:2304.07193 (2023)
32. Pai, J., Achenbach, L., Montesinos, V., Forrai, B., Mees, O., Nava, E.: mimic-video: Video-action models for generalizable robot control beyond vlas. arXiv preprint arXiv:2512.15692 (2025)
33. Qu, D., Song, H., Chen, Q., Yao, Y., Ye, X., Ding, Y., Wang, Z., Gu, J., Zhao, B., Wang, D., et al.: Spatialvla: Exploring spatial representations for visual-language-action model. arXiv preprint arXiv:2501.15830 (2025)
34. Sun, L., Xie, B., Liu, Y., Shi, H., Wang, T., Cao, J.: Geovla: Empowering 3d representations in vision-language-action models. arXiv preprint arXiv:2508.09071 (2025)
35. Wang, J., Chen, M., Karaev, N., Vedaldi, A., Rupprecht, C., Novotny, D.: Vggt: Visual geometry grounded transformer. In: Proceedings of the Computer Vision and Pattern Recognition Conference. pp. 5294–5306 (2025)
36. Wen, J., Zhu, M., Zhu, Y., Tang, Z., Li, J., Zhou, Z., Li, C., Liu, X., Peng, Y., Shen, C., et al.: Diffusion-vla: Generalizable and interpretable robot foundation model via self-generated reasoning. arXiv preprint arXiv:2412.03293 (2024)
37. Wen, J., Zhu, Y., Li, J., Zhu, M., Tang, Z., Wu, K., Xu, Z., Liu, N., Cheng, R., Shen, C., et al.: Tinyvla: Towards fast, data-efficient vision-language-action models for robotic manipulation. IEEE Robotics and Automation Letters (2025)
38. Won, J., Lee, K., Jang, H., Kim, D., Shin, J.: Dual-stream diffusion for world-model augmented vision-language-action model. arXiv preprint arXiv:2510.27607 (2025)
39. Xu, C., Zhang, S., Liu, Y., Sun, B., Chen, W., Xu, B., Liu, Q., Wang, J., Wang, S., Luo, S., et al.: An anatomy of vision-language-action models: From modules to milestones and challenges. arXiv preprint arXiv:2512.11362 (2025)
40. Yuan, T., Liu, Y., Lu, C., Chen, Z., Jiang, T., Zhao, H.: Depthvla: Enhancing vision-language-action models with depth-aware spatial reasoning. arXiv preprint arXiv:2510.13375 (2025)
41. Zhang, J., Chen, Y., Xu, Y., Huang, Z., Zhou, Y., Yuan, Y.J., Cai, X., Huang, G., Quan, X., Xu, H., et al.: 4d-vla: Spatiotemporal vision-language-action pretraining with cross-scene calibration. arXiv preprint arXiv:2506.22242 (2025)
42. Zhang, L., Rao, A., Agrawala, M.: Adding conditional control to text-to-image diffusion models. In: Proceedings of the IEEE/CVF international conference on computer vision. pp. 3836–3847 (2023)
43. Zhang, P.F., Cheng, Y., Sun, X., Wang, S., Li, F., Zhu, L., Shen, H.T.: A step toward world models: A survey on robotic manipulation. arXiv preprint arXiv:2511.02097 (2025)
44. Zhang, Z., Li, H., Dai, Y., Zhu, Z., Zhou, L., Liu, C., Wang, D., Tay, F.E., Chen, S., Liu, Z., et al.: From spatial to actions: Grounding vision-language-action model in spatial foundation priors. arXiv preprint arXiv:2510.17439 (2025)

45. Zheng, R., Liang, Y., Huang, S., Gao, J., Daumé III, H., Kolobov, A., Huang, F., Yang, J.: Tracevla: Visual trace prompting enhances spatial-temporal awareness for generalist robotic policies. arXiv preprint arXiv:2412.10345 (2024)
46. Zhou, H., Ma, C., Lee, G.H.: Vla-4d: Embedding 4d awareness into vision-language-action models for spatiotemporally coherent robotic manipulation. arXiv preprint arXiv:2511.17199 (2025)
47. Zhu, F., Yan, Z., Hong, Z., Shou, Q., Ma, X., Guo, S.: Wmpo: World model-based policy optimization for vision-language-action models. arXiv preprint arXiv:2511.09515 (2025)
48. Zitkovich, B., Yu, T., Xu, S., Xu, P., Xiao, T., Xia, F., Wu, J., Wohlhart, P., Welker, S., Wahid, A., et al.: Rt-2: Vision-language-action models transfer web knowledge to robotic control. In: Conference on Robot Learning. pp. 2165–2183. PMLR (2023)

## A Implementation Details of All Variants

This section summarizes the implementation details of the baseline and all compared injection variants, organized into architectures, training setup, and cost-related statistics.

### A.1 architectures

*Baseline and shared policy interface.* All variants share the same GR00T-N1.5 policy interface. The policy takes RGB observations from three views (an environment camera, a left wrist camera, and a right wrist camera) together with the robot state, and predicts an action chunk of horizon 16. In the standard GR00T pathway, the visual input consists of the current frame only from each view, with raw resolution  $480 \times 640 \times 3$  per image, resized to the input resolution required by the pretrained language-vision backbone. The state input also uses the current timestep only. Both state and action are represented in joint space rather than end-effector pose: each is 14-dimensional, comprising 6 arm-joint variables and 1 gripper variable for each arm. In the policy interface, state and action are padded to 64 and 32 dimensions, respectively. The baseline uses this standard pipeline without any auxiliary V-JEPA2 pathway.

*V-JEPA2 encoder.* For the injection-method comparison, the auxiliary visual encoder is a frozen V-JEPA2 model. Its input consists of temporally sampled history frames from three camera views; when the sampled history extends beyond the valid episode range, out-of-range indices are padded by repeating the nearest available frame. For each sample, the raw video is organized as  $[V, T, 480, 640, 3]$ , where  $V = 3$  is the number of views and  $T$  is the number of sampled history frames. The video is converted to floating point in  $[0, 1]$ , resized following the V-JEPA2 preprocessing rule (short side resized to 438), center-cropped to  $384 \times 384$ , and normalized using ImageNet statistics. After preprocessing, the encoder input is arranged as  $[B, V, C, T, 384, 384]$  and reshaped to  $[B \times V, C, T, 384, 384]$  before being fed into the frozen V-JEPA2 encoder. The encoder outputs patch-level visual features of shape  $[B \times V, N_{\text{patches}}, 1408]$ . In the main comparison of Sec. 4.1, we set  $T = 8$  and sample frames at 4 FPS.

*DINOv2 encoder.* For the encoder comparison in Sec. 4.2, we replace V-JEPA2 with a frozen DINOv2-Giant image encoder. Given the preprocessed visual tensor  $[B, V, C, T, 384, 384]$ , we extract the current frame (i.e., the last frame along the temporal dimension) to form  $[B, V, C, 384, 384]$ , reshape it to  $[B \times V, C, 384, 384]$ , and feed it into the frozen DINOv2-Giant encoder. We use the patch tokens from the last hidden state, excluding the CLS token, which yields features of shape  $[B \times V, N_{\text{patches}}, 1536]$ . These features are reshaped to  $[B, V \times N_{\text{patches}}, 1536]$  for subsequent projection and injection.

*Implementation differences across injection variants.* Across the compared injection variants, all methods use an additional projector to map auxiliary features into the action-expert interface, but the target dimension depends on the injection design. PVI, Concat, and ControlVLA-style project the auxiliary features from 1408 to the 2048-dimensional cross-attention space, whereas ControlNet-style and ReferenceNet-style project them to the 1536-dimensional DiT hidden space. PVI, ControlNet-style, and ReferenceNet-style additionally introduce a copied DiT-based branch initialized from the pretrained main DiT, while Concat and ControlVLA-style do not use an extra copied branch. The main DiT remains frozen in PVI and ControlNet-style, but is jointly trained in Concat, ReferenceNet-style, and ControlVLA-style.

## A.2 Training Setup

Unless otherwise specified, all experiments are initialized from the same pre-trained GR00T-N1.5-3B checkpoint. For the comparisons in Secs. 4.1–4.3, we follow the GR00T recommended fine-tuning schedules, using learning rate  $1 \times 10^{-4}$  and batch size 32 on 4 NVIDIA H20Z GPUs. Standard tasks are trained for 20k steps, while longer-horizon tasks are trained for 60k steps. Within each comparison, the baseline and all compared injection variants use exactly the same training schedule.

For the more challenging multi-task and real-robot experiments in Secs. 4.4–4.5, we use a longer training schedule of about 60 epochs with learning rate  $1 \times 10^{-4}$  and batch size 64 on 8 NVIDIA H20Z GPUs.

## A.3 Cost-Related Statistics

Tables 3, 4, and 5 report module-wise parameter breakdowns for the main injection-method comparison and the encoder comparison. We distinguish *trainable* and *total* parameter counts, since they reflect different costs: the former is more directly related to the optimization budget, while the latter also includes frozen auxiliary modules.

For the main injection-method comparison, PVI keeps the trainable budget comparable to, and in our case lower than, standard GR00T-N1.5 fine-tuning (901.73M vs. 1068.81M), even though it introduces an auxiliary encoder and an additional plug-in branch. This is because PVI freezes the original main DiT and places the newly introduced trainable capacity in the plug-in pathway, rather than increasing the optimized portion of the pretrained backbone. Importantly, PVI is trained in a single stage directly from the pretrained GR00T-N1.5 checkpoint, without requiring a separate “first fine-tune GR00T-N1.5, then fine-tune PVI” procedure. Therefore, in terms of trainable optimization budget, PVI does not require a larger fine-tuning budget than the standard baseline, while providing substantial performance gains.

By contrast, variants that continue to fine-tune the original main DiT, such as Concat and ControlVLA-style, remain at baseline-level trainable cost, while ReferenceNet-style becomes substantially heavier because it jointly trains both

the main DiT and an additional copied branch. In this sense, the parameter increase introduced by PVI should be interpreted mainly as the cost of attaching an external visual pathway, rather than of enlarging the trainable core of the original policy.

A similar pattern appears in the encoder comparison. Under the same PVI framework, replacing V-JEPA2 with DINOv2 or with the dual-encoder combination changes the trainable budget only marginally (901.73M, 901.99M, and 904.88M, respectively). The main increase is in total parameters, which is dominated by the frozen auxiliary encoder(s), while the trainable plug-in pathway remains nearly unchanged. This indicates that the cost difference across encoder choices primarily comes from the frozen visual frontend, rather than from a substantially larger optimized policy.

**Table 3: Parameter breakdown for the main injection-method comparison in Sec. 4.1 (Part I).** All numbers are in billions of parameters (B).

Quantity	Baseline		PVI		Concat	
	Trainable	Total	Trainable	Total	Trainable	Total
VLM	0.000	1.655	0.000	1.655	0.000	1.655
Main DiT	0.550	0.550	0.000	0.550	0.550	0.550
Others	0.518	0.518	0.317	0.518	0.518	0.518
Aux encoder	0.000	0.000	0.000	1.012	0.000	1.012
Plug-in branch	0.000	0.000	0.585	0.591	0.003	0.003
Total model	1.069	2.724	<b>0.902</b>	4.327	1.072	3.739
Trainable ratio	39.23%		<b>20.84%</b>		28.66%	

**Table 4: Parameter breakdown for the main injection-method comparison in Sec. 4.1 (Part II).** All numbers are in billions of parameters (B).

Quantity	ControlVLA-style		ControlNet-style		ReferenceNet-style	
	Trainable	Total	Trainable	Total	Trainable	Total
VLM	0.000	1.655	0.000	1.655	0.000	1.655
Main DiT	0.550	0.550	0.000	0.550	0.550	0.550
Others	0.518	0.518	0.317	0.518	0.317	0.518
Aux encoder	0.000	1.012	0.000	1.012	0.000	1.012
Plug-in branch	0.062	0.062	0.586	0.593	0.571	0.578
Total model	1.130	3.798	0.903	4.329	1.439	4.314
Trainable ratio	29.76%		20.87%		33.35%	

**Table 5: Parameter breakdown for the encoder comparison in Sec. 4.2.** All numbers are in billions of parameters (B).

Quantity	PVI@V-JEPA2		PVI@DINOv2		PVI@DINOv2+V-JEPA2	
	Trainable	Total	Trainable	Total	Trainable	Total
VLM	0.000	1.655	0.000	1.655	0.000	1.655
Main DiT	0.000	0.550	0.000	0.550	0.000	0.550
Others	0.317	0.518	0.317	0.518	0.317	0.518
Aux encoder	0.000	1.012	0.000	1.136	0.000	2.149
Plug-in branch	0.585	0.591	0.585	0.591	0.588	0.594
Total model	0.902	4.327	0.902	4.452	0.905	5.467
Trainable ratio	20.84%		20.26%		16.55%	

## B Full Multi-Task Per-Task Results

This section provides the full per-task results corresponding to Sec. 4.4 in the main paper. We report success rates over 100 rollouts for each task in the 20-task and 50-task RoboTwin 2.0 mixtures, where both the fine-tuned GR00T N1.5 baseline and GR00T N1.5 + PVI are trained with 50 demonstrations per task from the same pretrained checkpoint.

As summarized in the main paper, PVI improves the average success rate from 61.15% to 69.15% on the 20-task mixture and from 61.32% to 63.56% on the 50-task mixture. For completeness, we list the full per-task results below. For readability, the 50-task results are split into two consecutive tables.

**Table 6: Per-task success rates on the 20-task mixture.** All policies are trained with 50 demonstrations per task and evaluated over 100 rollouts per task. PVI improves the average success rate from 61.15% to 69.15% (+8.00 pp).

<b>Task</b>	<b>Baseline</b>	<b>PVI</b>
adjust_bottle	100%	99%
beat_block_hammer	67%	96%
click_alarmclock	88%	99%
move_can_pot	54%	52%
click_bell	99%	97%
move_playingcard_away	61%	73%
pick_diverse_bottles	18%	60%
place_a2b_left	52%	56%
open_laptop	68%	94%
press_stapler	79%	84%
rotate_qrcode	64%	63%
scan_object	41%	58%
put_object_cabinet	53%	62%
turn_switch	31%	60%
handover_block	70%	75%
open_microwave	17%	16%
stack_blocks_two	70%	63%
stack_bowls_two	95%	85%
blocks_ranking_rgb	69%	64%
blocks_ranking_size	27%	27%
<b>Average</b>	<b>61.15%</b>	<b>69.15% (+8.00 pp)</b>

**Table 7: Per-task success rates on the 50-task mixture (Part I).** All policies are trained with 50 demonstrations per task and evaluated over 100 rollouts per task. Across the full 50-task mixture, PVI improves the average success rate from 61.32% to 63.56% (+2.24 pp), outperforming the fine-tuned GR00T N1.5 baseline on 32 of 50 tasks and tying on 2 tasks.

Task	Baseline	PVI
adjust_bottle	99%	100%
beat_block_hammer	43%	86%
click_alarmclock	85%	93%
move_can_pot	43%	51%
click_bell	98%	98%
move_playingcard_away	64%	90%
pick_diverse_bottles	48%	68%
place_a2b_left	59%	52%
open_laptop	69%	94%
press_stapler	92%	89%
rotate_qrcode	56%	63%
scan_object	57%	56%
put_object_cabinet	73%	62%
turn_switch	32%	68%
handover_block	56%	67%
open_microwave	19%	20%
stack_blocks_two	75%	48%
stack_bowls_two	84%	93%
blocks_ranking_rgb	81%	55%
blocks_ranking_size	38%	19%
dump_bin_bigbin	88%	91%
grab_roller	100%	98%
handover_mic	97%	97%
hanging_mug	14%	19%
lift_pot	63%	84%

**Table 8: Per-task success rates on the 50-task mixture (Part II).**

Task	Baseline	PVI
move_stapler_pad	6%	8%
move_pillbottle_pad	39%	63%
pick_dual_bottles	46%	62%
place_a2b_right	56%	38%
place_bread_basket	67%	61%
place_bread_skillet	53%	56%
place_burger_fries	95%	59%
place_can_basket	52%	57%
place_cans_plasticbox	70%	71%
place_container_plate	91%	96%
place_dual_shoes	38%	46%
place_empty_cup	79%	88%
place_fan	29%	33%
place_mouse_pad	26%	22%
place_object_basket	76%	62%
place_object_scale	46%	31%
place_object_stand	66%	67%
place_phone_stand	69%	72%
place_shoe	55%	68%
put_bottles_dustbin	48%	53%
shake_bottle_horizontally	99%	100%
shake_bottle	96%	100%
stack_blocks_three	32%	13%
stack_bowls_three	71%	51%
stamp_seal	28%	40%
<b>Average</b>	<b>61.32%</b>	<b>63.56% (+2.24 pp)</b>